Eurasian Journal of Soil Science 2022, 11(2), 102 - 112

Eurasian Journal of Soil Science

Journal homepage : http://ejss.fesss.org

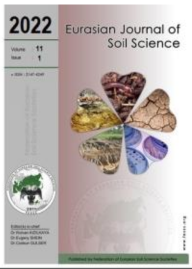

Spatial modeling of soil salinity using kriging interpolation techniques: A study case in the Great Hungarian Plain

Ghada Sahbeni *, Balázs Székely

Department of Geophysics and Space Science, Eötvös Loránd University, Budapest, Hungary

Article Info

Received : 21.04.2021
Accepted : 18.10.2021
Available online : 22.10.2021

Author(s)

G.Sahbeni *
B.Székely

* Corresponding author

Abstract

The world's current task is to ensure food security for an ever-growing population of 7.674 billion in 2019. Soil degradation threatens sustainable agriculture in arid and semi-arid climates, where evaporation rates outweigh precipitation. Soluble salts concentrated in the subsoil under certain climatic conditions influence soil physicochemical properties, leading to soil fertility and biodiversity losses. Hence, understanding salinity behavior and its spatial variation are crucial for natural resources management to achieve and maintain sustainability. This study aims to model soil salinity spatial distribution using four kriging interpolation methods, i.e., ordinary kriging (OK), empirical Bayesian kriging (EBK), co-kriging (CK), and indicator kriging (IK). Two hundred twenty-two soil samples were collected for this purpose during a field campaign conducted in the Hungarian Soil Monitoring System framework in 2016. The performance of kriging methods was assessed and compared using two cross-validations, i.e., leave-one-out cross-validation (LOOCV) and the holdout method. The Pearson correlation analysis has been used to expose a significant moderate correlation between salt content and cation exchange capacity (CEC) with a correlation coefficient of 0.4 and a p-value of 0.003. Thus, the spatial relationship between soil salinity content (SSC) and CEC was integrated into the model to enhance predictions in areas where no measurements were accessible. The study demonstrated co-kriging efficiency by reducing the mean squared error (MSE) of ordinary kriging (OK) from 0.8 g/kg and 0.85 g/kg for LOOCV and the holdout cross-validation to 0.3 g/kg.

Keywords: Geostatistics, interpolation, kriging, soil salinity, spatial modeling.

Introduction

The accumulation of salts in the subsurface and rhizosphere, known as salinization, leads to degraded soil composition and reduced crop yield, threatening food security (Shahid et al., 2018). The global surface area affected by salinization covers approximately 831 million hectares, with 434 million hectares as sodic soils and 397 million hectares as saline soils. There are two forms of salinization based on occurrence causes. Primary salinization originates from parent material weathering, while anthropogenic actions induce secondary salinization (Uri, 2018). Extensive work using field measurements coupled with remote sensing tools, statistical analysis, geostatistics, and machine learning has been conducted to map and monitor salt-affected lands expansion over time. Many researchers have explored this topic, including Taghadosi et al. (2019), El hafyani et al. (2019), Hoa et al. (2019), Abdel-Fattah et al. (2020), and Sahbeni (2021). Geostatistical analysis generates an estimated surface from a distributed set of points using various methods, e.g., kriging, nearest neighbor, spline, inverse distance weighting (IDW), global polynomial interpolation (GPI), and conditional simulations (Emadi and Baghernejad, 2014; Sangani et al., 2019). Kriging interpolation was used by Panday et al. (2018) to determine soil chemical properties distribution over agricultural floodplain lands of the Bara district in Nepal. The study revealed a moderate spatial

: https://doi.org/10.18393/ejss.1013432
: http://ejss.fesss.org/10.18393/ejss.1013432
Publisher : Federation of Eurasian Soil Science Societies
e-ISSN : 2147-4249

variability for pH, organic matter, nitrogen, and phosphorus. Farmers can analyze soil quality and adopt appropriate agricultural production methods based on developed maps. Abdennour et al. (2019) applied ordinary kriging (OK) and indicator kriging (IK) for salinity levels analysis in the irrigated perimeter of El-Ghrous in south-eastern Algeria. The research has determined salinity trends based on different classes and has created risk maps that decision-makers could employ in the region. Tziachris et al. (2017) compared ordinary kriging, universal kriging, and co-kriging to estimate iron content in the Kozani area. An outperformance of the co-kriging method was revealed by adding soil pH as an auxiliary variable to enhance predictions in unsampled areas. Nie et al. (2021) used kriging interpolation to study secondary salinization extent over agricultural areas in the western Jilin irrigation district, northeast China. The results showed an improvement in accuracy by 23.2% using geographically weighted regression kriging (GWRK) compared to regression kriging (RK). This provides a theoretical perspective for controlling groundwater to regulate soil salinity and prevent salinization through quantitative analysis via kriging.

The Great Hungarian Plain occupies more than 50% of Hungary's total surface, and it is contaminated by soil and wetland salinization (Mádl-Szőnyi et al., 2008). Salt content, hydraulic properties of soil, and the watertable depth influence salt-affected soils genesis in Hungary (Schofield et al., 2001), where saline soils cover 6% of its territory, making it one of the largest natural areas in Europe affected by primary salinization (Tóth et al., 2008). Thus, this expansion has inspired Hungarian scientists to study salinity behavior, origins, and restoration programs in the last decades (Tóth, 2009; Csillag et al., 1993; Tóth et al., 2002; Szatmári et al., 2020). Salinization mapping has become a valuable task for developing appropriate reclamation strategies to preserve soil quality and sustain agricultural productivity in the region. This study aims to (1) use field measurements to map salinity spatial distribution in the Great Hungarian Plain and (2) compare the predictive performance of four kriging methods, namely ordinary kriging (OK), empirical Bayesian kriging (EBK), co-kriging (CK), and indicator kriging (IK).

Material and Methods

Study area

The study area covers approximately 26300 km^2 (Figure 1), with an average altitude of 89 meters (Figure 2). Meadow chernozems and humic sandy soils dominate the landscape with an expanded agricultural land cover (Pásztor et al., 2018). The river Tisza crosses the study area, gathering tributaries from the surrounding floodplains. (Tóth et al., 2014). A warm-dry climate characterizes the study area, with an average yearly precipitation of roughly 500 mm and a mean temperature of 11°C (Hungarian Meteorological Service, 2018). May and July are the rainiest months, while January and March are the driest. Three types of deposits dominate the landscape: loess and loess-like sediments above the floodplains, silty clay in alluvial areas, and wind-blown sand on the slopes (Ronai, 1986).

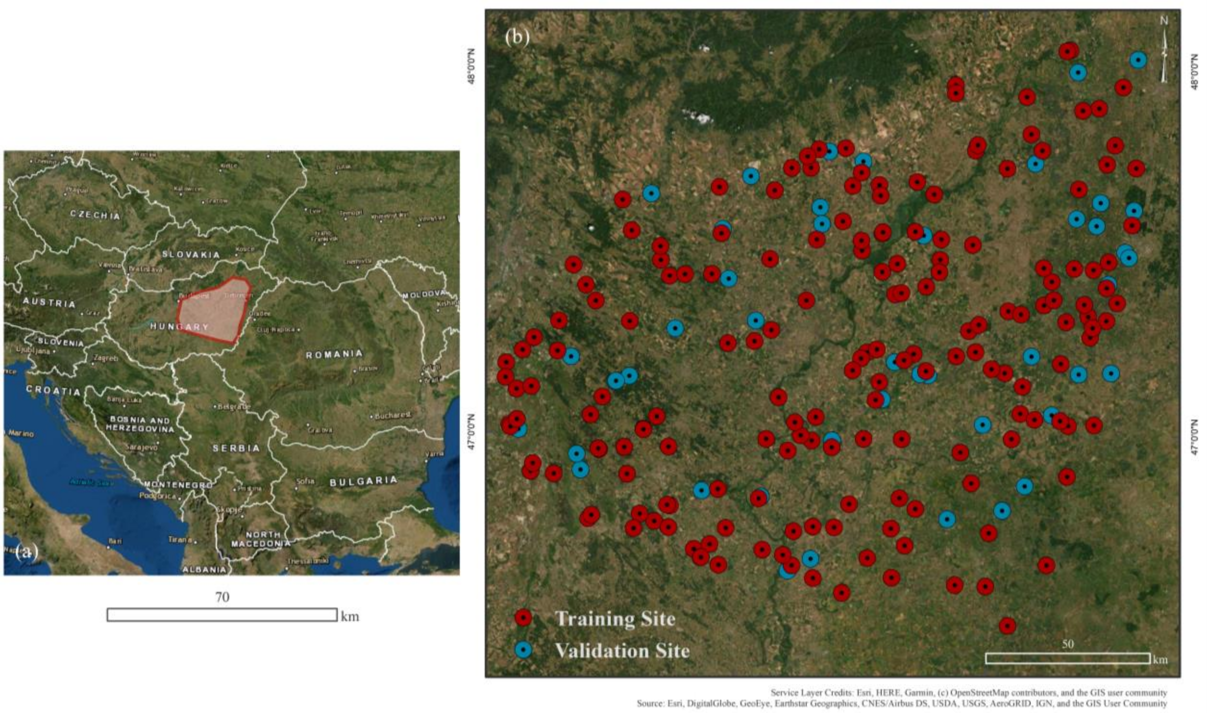

Figure 1. The study area's geographical location; (a) Satellite imagery map using ESRI basemap in ArcMap 10.3; (b) Location of sampling sites

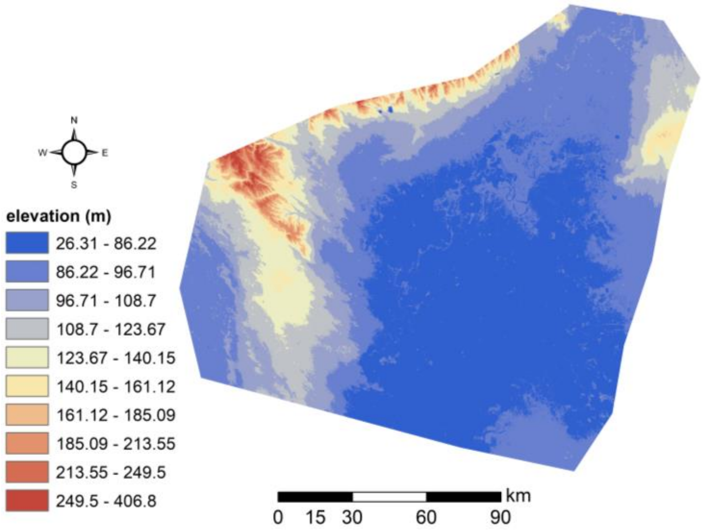

Figure 2. Altitude map of the study area using a 30-m SRTM digital elevation model provided by the OpenTopography facility.

Soil Sampling and Laboratory Analysis

From mid-September to mid-October 2016, 222 soil samples were collected within the soil upper layer (30 cm) in the Hungarian Soil Monitoring System framework. The field survey is conducted in the dry season to detect the spectral properties of salts during their accumulation (Szabó and Pirkó, 2017). The Hungarian standard MSZ-08-0206/2-1978 is used to calculate soil salinity from saturated paste (MSZ 08-0206-2, 1978).

Semivariogram Modeling

The first step in kriging interpolation is to estimate an experimental semivariogram for the parameter to be modeled. Equation (1) illustrates the semivariance expression (Deutsch and Journel, 1998).

$$\gamma(h) = \frac{1}{2N(h)} \, x \sum_{i}^{N(h)} [Z(s_i) - Z(s_i + h)]^2 \tag{1}$$

Where s_i is the location of the i[th] sample,
$Z(s_i)$ is the measurement,
h is the distance between $Z(s_i)$ and $Z(s_i + h)$, and
$N(h)$ is the number of pairs $Z(s_i)$ over the distance h.

A semivariogram depicts the estimated $\gamma(h)$ against h values plot (Tziachris et al., 2017). Its main parameters are range, sill, partial sill, and nugget. The range (A) represents the distance to the semivariogram flattening. The sill (C) is the y-value of the model at the range, whereas the partial sill (C_1) is the difference between the sill and the nugget (C_0), which is the random spatial variation (Hartmann et al., 2018; Guedes et al., 2020). The spatial dependency can be measured by dividing the nugget over the sill ratio ($C_0/(C_0 + C_1)$). A value below 25% implies severe spatial dependence, a value within 25% and 75% range represents mild spatial dependence, while a value more than 75% represents weak dependence (Cambardella et al., 1994). Figure 3 shows the structure of a semivariogram model.

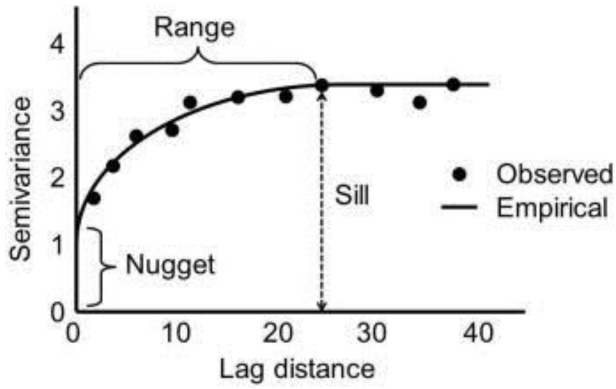

Figure 3. Typical structure of a semivariogram model (Biswas and Si, 2013)

Several model functions can be used to estimate experimental semivariograms in applied geostatistics, such as circular, spherical, exponential, gaussian, and linear (Smith, 2011). Once a model is fitted, cross-validation is conducted to evaluate the performance of the kriging method. In this context, we used samples from a random training set representing 70% of the total data to build experimental semivariogram models, while 30% of the samples were used for validation.

Kriging Interpolation

Kriging interpolation, named after Danie Krige, is a geostatistical approach for estimating unknown values based on the distance and the degree of variation between data points (Krige, 1985; Zhang, 2011; Thompson et al., 2012). A kriged estimate refers to the weighted linear combination of known values near the estimated locations. It helps produce weights resulting in optimum and unbiased estimates (Wackernagel, 2013; Xiao et al., 2016). We estimate $\hat{Z}(s_0)$ at unknown s_0 locations after measuring N data values, $Z(s_1)$, $Z(s_2)$,..., $Z(s_N)$ at s_1, s_2,..., s_N locations. $Z(s_i)$ represents the estimated value at the s_i location, whereas λ_i represents the unknown weight for the measured value at the s_i location. $\hat{Z}(s_0)$ is computed using Equation (2).

$$\hat{Z}(s_0) = \sum_{i=1}^{N} \lambda_i \text{ x } Z(s_i) \tag{2}$$

This step aims to find the weights λ_i to minimize the variance Var[$\hat{Z}(s_0) - Z(s_0)$].

Given that the estimator is assumed to be unbiased:

$$E[\,\hat{Z}(s_0)\; - \;Z(s_0)] \; = \; 0 \tag{3}$$

$\hat{Z}(s_0)$ is separated into two parts: a trend component $m(s_0)$ and a residual component $e(s_0)$, as shown in Equation (4).

$$\hat{Z}\,(s_0) \; = \; m(s_0) \; + \; e(s_0) \tag{4}$$

We employed ArcMap 10.3 to conduct interpolations and to evaluate the efficiency of ordinary kriging (OK), indicator kriging (IK), empirical Bayesian kriging (EBK), and co-kriging (CK) in terms of salt content prediction throughout cross-validation. Ordinary kriging is a spatial prediction approach that reduces error variance through data configuration and variogram fitting (Wackernagel, 1995). This technique has been well presented by many scholars, i.e., Negreiros et al. (2010), Hamzehpour et al. (2013), and Kiš (2016). Indicator kriging estimates a conditional cumulative distribution function at unsampled locations using spatial interpolation. It uses indicator variables to determine the likelihood of a crucial value being overridden or not at each point in the region of interest (Delbari et al., 2011; Pásztor et al., 2015). While other methods require a manual configuration to get reliable results, empirical Bayesian kriging (EBK) automates the most exigent elements to build a realistic kriging model, making it easier to obtain more accurate predictions. These parameters are estimated using a simulation algorithm. It involves little interactive modeling but produces better results for small datasets, outperforming other kriging approaches in terms of standard errors (Bhunia et al., 2016; Samsonova et al., 2017; Gribov and Krivoruchko, 2020). Co-kriging is a multivariate form of ordinary kriging that uses a well-sampled variable to estimate a poorly sampled one, considering primarily significant associations (Tajgardan et al., 2010; Gräler, 2011**;** Babiker et al., 2018). For this purpose, we downloaded Landsat-8 OLI data acquired in August 2016. The multispectral data were atmospherically and radiometrically corrected via ENVI IDL 5.3. We computed the canopy response salinity index (CRSI) (Scudiero et al., 2017) and albedo (Silva et al., 2016). Principal component analysis (PCA) was applied to reduce the sensor spectral noise, then only the first and the second components were extracted as they contain 98% of data variance. Additionally, slope, profile curvature, and wetness index were derived from an SRTM digital elevation model (DTM), provided by OpenTopography Facility, using ArcMap 10.3. Cation Exchange Capacity (CEC) raster data were retrieved from the European Soil Database v2 Raster Library 1 km × 1 km, provided by the European Soil Data Centre (ESDAC) (Panagos et al., 2012, ESDAC, 2021). Once remotely sensed data were processed and corresponding values to samples were extracted, Pearson correlation was conducted using RStudio 1.4.1106 to outline the potential relationship between salt content values and spectral response.

Cross-validation

Two cross-validation methods were used to compare the four state-of-the-art methods. The leave-one-out cross-validation (LOOCV) method predicts using a single observation from the training set, while the left-out observations are used to train the model. Holdout cross-validation divides the data set randomly into 70% for training and 30% for validation. We calculated the mean squared error (MSE) and the mean absolute error (MAE) for LOOCV, while the root mean square error (RMSE) and the mean squared error (MSE) for holdout cross-validation. Equations (5), (6), and (7) illustrate statistical metrics expressions.

$$RMSE = \sqrt{\sum_1^n (\hat{y}_i - y_i)^2 / n} \tag{5}$$

$$\mathrm{MSE} = \frac{1}{n} \times \sum (y_i - \hat{y}_i)^2 \tag{6}$$

$$\mathrm{MAE} = \frac{1}{n} \times \sum_1^n |y_i - \hat{y}_i| \tag{7}$$

Where n is the total number of observations, $\hat{y}_i$ is the estimated value for the i^{th} observation, and y_i is the actual value for the i^{th} observation.

Results

Exploratory Data Analysis

Table 1 shows the key statistical parameters of field data. Salinity distribution is characterized by a mean of 0.54 g/kg and a standard deviation of 0.85 g/kg. The substantial difference between a minimum of 0 g/kg and a maximum of 8.5 g/kg indicates a wide spatial variability of this parameter.

Table 1. Descriptive statistics of salt content samples

	Min	Max	Mean	Standard Deviation
Salt Content (g/kg)	0	8.5	0.54	0.85

The regression analysis revealed a significant moderate association between salt content and CEC, with a correlation coefficient of 0.4 and a p-value of 0.003 (< 5%). This positive correlation was discussed by previous studies (Shainberg et al., 1980; Naseem and Bhatti, 2000). Figure 4 shows the correlation coefficients between salt content and auxiliary variables.

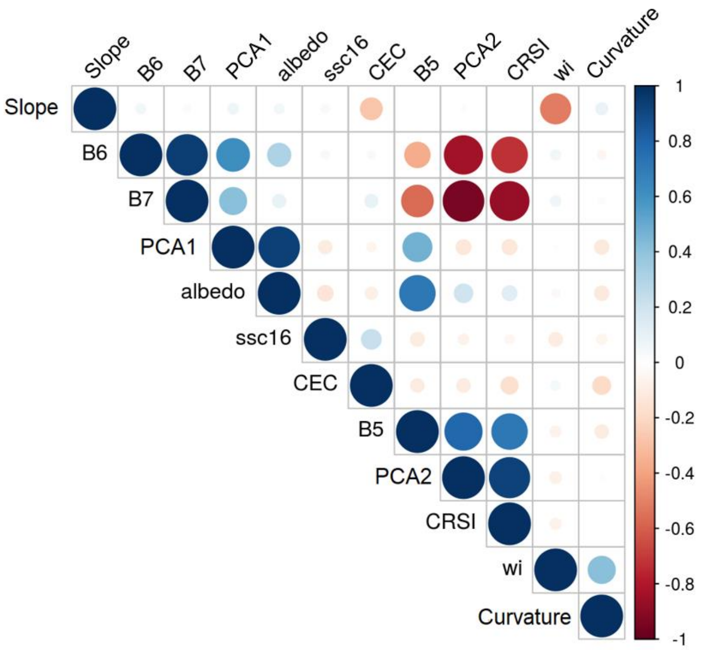

Figure 4. Correlation between soil salinity content and auxiliary covariates, where ssc16 refers to soil salinity content in 2016. B5, B6, and B7 are spectral bands retrieved from Landsat-8 OLI data, while PCA1 and PCA2 are the first and the second principal components of the same image. CRSI is the Canopy Response Salinity Index. Wetness index (wi), slope, and curvature are derived from a 30-m SRTM Digital Elevation Model (DEM).

Analysis of Semivariograms

A semivariogram describes spatial autocorrelation between measured salt content values. Features can be extracted to define each model once it is fitted across each pair of observations. Table 2 and Figure 5 summarize the findings.

Indicator kriging has a high range of 11332.56 m, followed by co-kriging with a range of 88458.18 m, respectively. The range is lower for ordinary kriging (= 5893.58 m) with a partial sill close to co-kriging (0.686 and 0.691). A high ratio of 32.1 % was found for co-kriging, revealing a moderate spatial dependence. The spatial dependence is strong for indicator kriging equals 18.5 %, whereas it is extreme for ordinary kriging with a ratio of 6.3 %.

Table 2. The semivariogram models and their parameters for kriging methods. The spatial dependence equals $C_0/(C_0+C_1)$.

	Model	Nugget (C_0)	Partial Sill (C_1)	Range (A) (m)	Dependence (%)
OK	Gaussian	0.046	0.686	5893.58	0.063
EBK	Exponential	***	***	***	***
CK	Gaussian	0.327	0.691	88458.18	0.321
IK	Gaussian	0.018	0.078	11332.56	0.185

*** For EBK, the semivariance is rather an empirical distribution than a fixed parameter. Therefore, spatial dependence cannot be estimated.

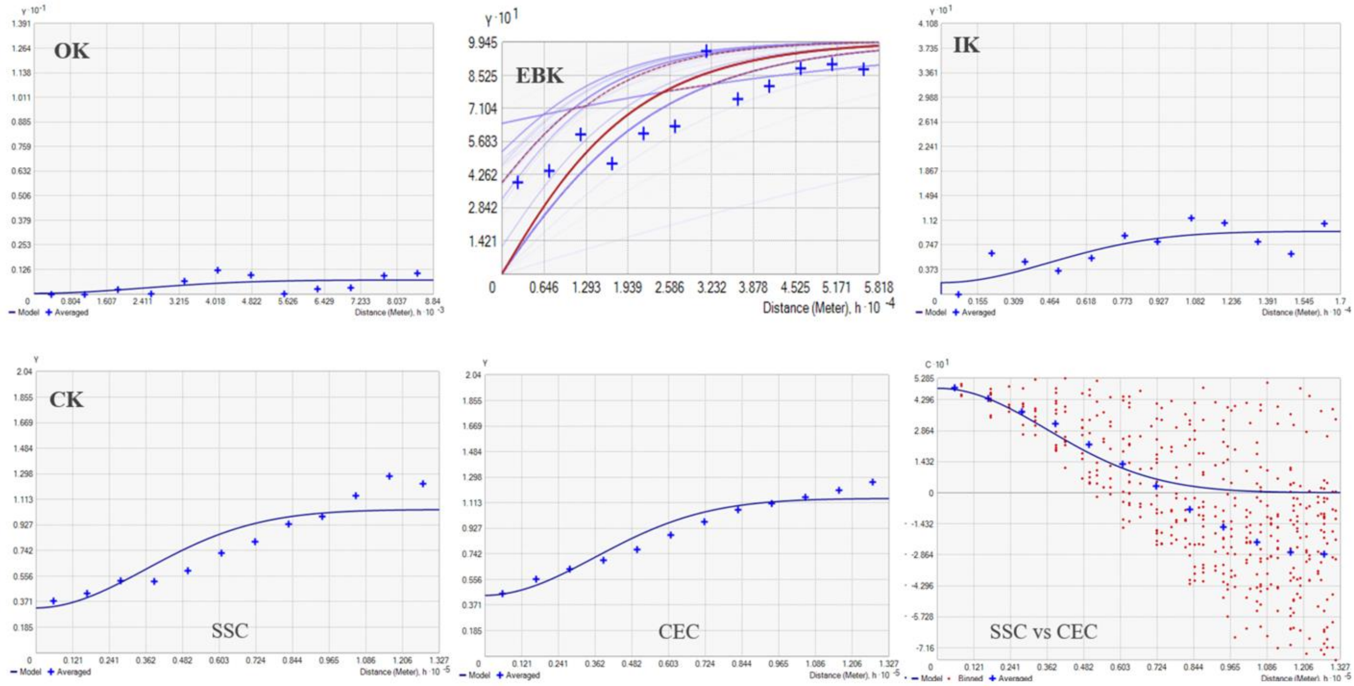

Figure 5. Semivariograms of soil salinity content (SSC) distribution and their fitted models

For empirical Bayesian kriging, these parameters are analyzed in empirical distributions. Since several semivariograms are measured at each site, these models have neither a range nor a sill.

Soil Salinity Prediction

Based on Figure 6, predictions revealed similar patterns with minor differences for kriging methods. Areas with higher salt content predictions are condensed in the east and the center of the study area (Orange color) on lower altitudes, whereas areas with lower predictions were found west of the river Tisza, on slightly higher altitudes.

Figure 7 shows that areas with higher prediction errors (Red color) are found in the study area center due to the sparse density of sampling sites in the river Tisza vicinity. Empirical Bayesian kriging produced the lowest prediction errors with a minimal disparity in the east and the center. Yet, co-kriging (CK) yielded better results compared to ordinary kriging (OK) in terms of prediction errors distribution. Errors are overestimated by empirical Bayesian kriging compared to co-kriging with maximum values equal to 1.07 and 0.36, respectively. Table 3 illustrates the results of leave-one-out cross-validation and holdout cross-validation.

Table 3. The results of cross-validation for soil salinity prediction. The Root Mean Square Error (RMSE), Mean Squared Error (MSE), and Mean Absolute Error (MAE), expressed in g/kg, were used to compare the performance of kriging models.

CV	Error	OK	EBK	CK	IK
Holdout Cross-Validation	RMSE	0.53	0.57	0.60	0.24
	MSE	0.85	0.49	0.30	0.30
LOOCV	MAE	0.18	0.18	0.22	0.02
	MSE	0.80	0.42	0.30	0.30

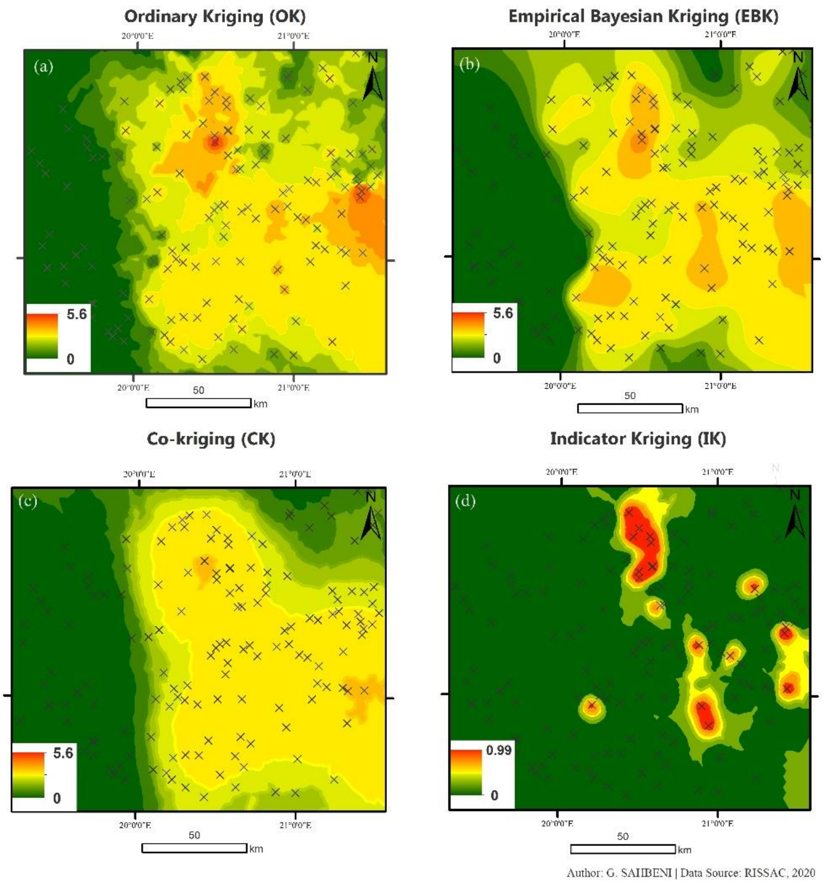

Figure 6. Prediction maps for salt content (g/kg) spatial distribution using kriging interpolation methods, (a) OK; (b) EBK; (c) CK; (d) IK

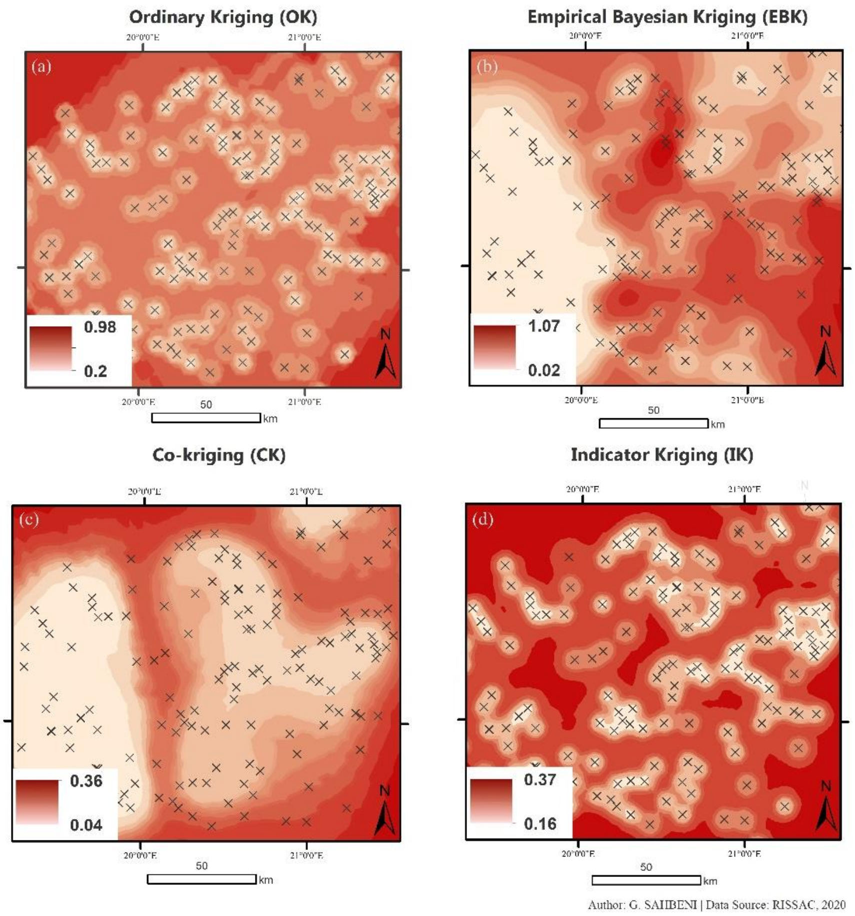

Figure 7. Prediction error maps of salt content (g/kg) spatial distribution using kriging interpolation methods, (a) OK; (b) EBK; (c) CK; (d) IK

Co-kriging and indicator kriging produced the lowest MSE (= 0.3 g/kg) for the holdout cross-validation and leave-one-out cross-validation. Meanwhile, ordinary kriging has the highest MSE for holdout cross-validation and LOOCV, equal to 0.53 g/kg and 0.8 g/kg, respectively. For RMSE, indicator kriging has the lowest value (= 0.24 g/kg), followed by ordinary kriging (= 0.53 g/kg), empirical Bayesian kriging (= 0.57 g/kg), and co-kriging (= 0.6 g/kg). For MAE, indicator kriging has the lowest value, equal to 0.02 g/kg, followed by ordinary kriging, empirical Bayesian kriging, and co-kriging. Overall, kriging methods have close RMSE and MAE values except for indicator kriging as it produces probabilities rather than numeric values.

Co-kriging performed well in terms of MSE reduction for both cross-validation stages compared to ordinary kriging. In contrast, empirical Bayesian kriging and indicator kriging showed better performance in terms of MAE, revealing a remarkable potential to produce unbiased predictions. The superiority of co-kriging was expected due to its hybrid structure, conditionally with a strong correlation between variables as the spatial distribution of one parameter is exploited to estimate the behavior of the second one. Despite the significant improvement of predictions using co-kriging, the correlation between salt content and CEC is moderate (40%), which limited the model from outperforming other methods in terms of RMSE. This issue can be investigated in future studies.

Discussion

This study demonstrates geostatistics efficiency in mapping salinity distribution with significant accuracy, supported by the studies of Gallichand et al. (1992) and Pulatov et al. (2020). Benslama et al. (2020) interpolated the electrical conductivity (EC) using inverse distance weighting (IDW) and ordinary Kriging (OK). Interpolation methods performed well in soil salinity mapping, with mean error (ME) and root mean square error (RMSE) of -0.003 dS/m and 0.145 dS/m, respectively. In the same context, Nezami and Alipour (2012) examined the potential of interpolation methods in salinity mapping across the Qazvin Plain, i.e., ordinary kriging (OK), co-kriging (CK), spline, and inverse distance weighted (IDW). The results revealed that co-kriging performed well due to the integration of clay content (%), with a root mean square error (RMSE) equal to 108 dS/m^2. This agrees with our findings regarding the outperformance of co-kriging in modeling salinity distribution with a prediction error ranges between 0.04 g/kg and 0.36 g/kg. The co-kriging model of Abdennour et al. (2020) yielded a root mean square error (RMSE) of 0.92 dS/m and a mean error (ME) of 0.004 dS/m, revealing an accuracy enhancement by adding saturation index (SI) of gypsum and SO_4^{2-}, NDVI, and terrain parameters. Using CEC as an auxiliary covariate, our cokriging model produced better predictions in terms of soil salinity modeling with a root mean squared error (RMSE) equals 0.6 g/kg and a mean squared error (MSE) equals 0.3 g/kg. However, more improvement can be made by including variables with stronger associations rather than the cation exchange capacity (CEC). Triantafilis et al. (2001) compared four kriging methods, i.e., ordinary kriging, regression kriging (RK), dimensional kriging (DK), and co-kriging (CK), using electromagnetic induction data across an irrigated cotton in the Namoi valley (Australia). Despite the superiority of regression kriging in precision and estimation bias, co-kriging produced more accurate predictions, supporting our findings. The ordinary kriging method performed well with an RMSE equal to 0.53 g/kg, agreeing with Nawar et al. (2011) study that revealed ordinary kriging potential based on a spherical semivariogram for mapping salinity distribution in El-Tina Plain (Egypt). Similarly, Zheng et al. (2009) predicted electrical conductivity (EC) variation in the west margin of Taklamakan desert using ordinary kriging (OK). The model produced an efficiency factor (E) of 0.7793 mS/cm and a prediction ratio to deviation (RPD) of 0.39 mS/cm. The study agrees with our findings regarding ordinary kriging efficiency as a promising alternative to spatially map salinity with acceptable accuracy.

An interpretation of prediction maps showed that higher salinity predictions are concentrated around lower altitudes around the river Tisza and Hortobágy National Park, whereas lower salinity predictions are frequent in slightly higher altitudes. Topography and climate play a crucial role in salt accumulation and movement within the subsoil, as discussed by many scholars (Schofield et al., 2001; Ivushkin et al., 2017; Sahbeni, 2021). Thus, it is recommended to adopt a practical field sampling approach that preserves the continuity and the representativeness principles. To produce more accurate results, distance between sites, sampling density, geologic formations, and topographic parameters of the study area must be considered.

Conclusion

The current study investigates kriging potential in salinity prediction. Implementing a suitable method that minimizes errors and predicts salt content accordingly offers a quick and affordable approach to monitoring salinity variation and preventing its expansion. In this context, co-kriging performed well in terms of prediction error distribution that varies between 0.04 g/kg and 0.36 g/kg using cation exchange capacity (CEC) as an auxiliary covariate. Stronger associations with soil salinity in the vicinity of unsampled or poorly sampled sites can improve co-kriging performance and reduce prediction error. On the other hand, indicator kriging outperformed other methods in terms of MSE, MAE, and RMSE, with values of 0.3 g/kg, 0.02 g/kg, and 0.24 g/kg for LOOCV and holdout cross-validation, respectively. We have found that more than 10% of the study area surpassed the 1g/kg threshold limit, which might require immediate intervention to validate this scenario. Overall, salinity distribution maps can assist in boosting awareness of reclamation programs for sustainable agriculture and implementing feasible planning strategies. Nevertheless, the sample size and the non-uniform distribution of samples affected prediction errors by overestimating or underestimating in areas where no or few samples were taken. Further research must be conducted on larger scales (agricultural lands/farms scale) to validate the applicability of the proposed approach.

Acknowledgements

The authors express their gratitude to Prof. L. Pásztor for his valuable support in acquiring field data from the Research Institute of Soil Science and Agricultural Chemistry (RISSAC). The authors would like to genuinely thank the editor and the anonymous reviewers for their constructive feedback to improve the manuscript quality.

References

Abdel-Fattah, M.K., 2020. A GIS-based approach to identify the spatial variability of salt affected soil properties and delineation of site-specific management zones: A case study from Egypt. *Soil Science Annual* 71(1): 76-85.

Abdennour, M.A., Douaoui, A., Bradaï, A., Bennacer, A., Fernández, M.P., 2019. Application of kriging techniques for assessing the salinity of irrigated soils: the case of El Ghrous perimeter, Biskra, Algeria. *Spanish Journal of Soil Science* 9(2): 105-124.

Abdennour, M.A., Douaoui, A., Piccini, C., Pulido, M., Bennacer, A., Bradaï, A., Barrena, J., Yahiaoui, I., 2020. Predictive mapping of soil electrical conductivity as a Proxy of soil salinity in south-east of Algeria. *Environmental and Sustainability Indicators* 8: 100087.

Babiker, S., Abulgasim, E., Hamid H.S., 2018. Enhancing the spatial variability of soil salinity ındicators by remote sensing indices and geo-statistical approach. *Journal of Earth Science & Climatic Change* 9: 1-7.

Benslama, A., Khanchoul, K., Benbrahim, F., Boubehziz, S., Chikhi, F., Navarro-Pedreño, J., 2020, Monitoring the variations of soil salinity in a palm grove in Southern Algeria. *Sustainability* 12(15): 6117.

Bhunia, G.S., Shit, P.K., Maiti, R., 2016. Comparison of GIS-based interpolation methods for spatial distribution of soil organic carbon (SOC). *Journal of the Saudi Society of Agricultural Sciences* 17(2): 114-126.

Biswas, A., Si, B.C., 2013. Model averaging for semivariogram model parameters. In: Advances in agrophysical research. Grundas, S., Stepniewski, A. (Eds.). IntechOpen. Available at [access date: 21.04.2021]: https://www.intechopen.com/chapters/39857

Cambardella, C., Moorman, T., Parkin, T., Karlen, D., Novak, J., Turco, R., Konopka, A., 1994. Field-scale variability of soil properties in central Iowa soils. *Soil Science Society of America Journal* 58: 1501–1511.

Csillag, F., Pásztor, L., Biehl L.L., 1993. Spectral band selection for the characterization of salinity status of soils. Remote Sensing of Environment 43(3): 231–242.

Delbari, M., Afrasiab, P., Loiskandl, W., 2011. Geostatistical analysis of soil texture fractions on the field scale. *Soil and Water Research* 6: 173-189.

Deutsch, C., Journel, A., 1998. Geostatistical software library and user's guide. Oxford University Press, Oxford. 369p.

El hafyani, M., Essahlaoui, A., El Baghdadi, M., Teodoro, A.C., Mohajane, M., El hmaidi, A., El ouali , A.,2019. Modeling and mapping of soil salinity in Tafilalet plain (Morocco). *Arabian Journal of Geosciences* 12: 35.

Emadi, M., Baghernejad, M., 2014. Comparison of spatial interpolation techniques for mapping soil pH and salinity in agricultural coastal areas, northern Iran. *Archives of Agronomy and Soil Science* 60(9): 1315-1327.

ESDAC, 2021. European Soil Data Centre (ESDAC). European Commission, Joint Research Centre. Available at [Access date: 21.04.2021]: https://esdac.jrc.ec.europa.eu/

Gallichand, J., Buckland, G.D., Marcotte, D., Hendry, M.J., 1992. Spatial interpolation of soil salinity and sodicity for a saline soil in Southern Alberta. *Canadian Journal of Soil Science* 72(4): 503-516.

Gräler, B., 2011. Cokriging and indicator kriging. Seminar Spatio-temporal dependence. University of Münster. Available at [Access date: 21.04.2021]: http://www.graeler.org/copulaIntro/02_Co-Kriging_Indicator-Kriging.pdf

Gribov, A., Krivoruchko, K., 2020. Empirical Bayesian kriging implementation and usage. *The Science of The Total Environment* 722: 137290.

Guedes, L.P., Bach, R.T., Uribe-Opazo, M.A., 2020. Nugget effect influence on spatial variability of agricultural data. *Engenharia Agrícola* 40(1): 96-104.

Hamzehpour, N., Eghbal, M.K., Bogaert, P., Toomanian, N., Sokouti, R.S., 2013. Spatial prediction of soil salinity using kriging with measurement errors and probabilistic soft data. *Arid Land Research and Management* 27(2): 128-139.

Hartmann, K., Krois, J., Waske, B., 2018. E-Learning Project SOGA: Statistics and Geospatial Data Analysis. Freie Universitaet Berlin. Available at [Access date: 21.04.2021]: https://www.geo.fu-berlin.de/en/v/soga/index.html

Hoa, P.V., Giang, N.V., Binh, N.A., Hai, L.V.H., Pham, T.D., Hasanlou, M., Bui, D.T, 2019. Soil salinity mapping using SAR Sentinel-1 data and advanced machine learning algorithms: A case study at Ben Tre Province of the Mekong River Delta (Vietnam). *Remote Sensing* 11(2): 128.

Hungarian Meteorological Service, 2018. Precipitation conditions of Hungary. Available at [Access date: 21.04.2021]: https://www.met.hu/en/eghajlat/magyarorszag_eghajlata/altalanos_eghajlati_jellemzes/csapadek/

Ivushkin, K., Bartholomeus, H., Bregt, A.K., Pulatov, A., 2017. Satellite thermography for soil salinity assessment of cropped areas in Uzbekistan. *Land Degradation and Development* 28(3): 870–877.

Kiš, M.I., 2016. Comparison of ordinary and universal kriging interpolation techniques on a depth variable (a case of linear spatial trend), case study of the Šandrovac field. *The Mining-Geological-Petroleum Bulletin* 31(2): 41–58.

Krige, D., 1985. The use of geostatistics in defining and reducing the uncertainty of grade estimates. *South African Journal of Geology* 88(1): 69-72.

Mádl-Szőnyi, J., Tóth, J., Pogácsás, G., 2008. Soil and wetland salinization in the framework of the Danube-Tisza Interfluve hydrogeologic type section. *Central European Geology* 51(3): 203-217.

MSZ 08-0206-2, 1978. Evaluation of some chemical properties of the soil. Laboratory tests. (pH value, phenolphtaleine alkalinity expressed in soda, all water-soluble salts, hydrolite (yˇ1^-value), and exchanging acidity (yˇ2^- value). Hungarian Standards Institution.

Naseem, I., Bhatti, H.N., 2000. Organic matter and salt concentration effect on cation exchange equilibria in non-calcareous soils. *Pakistan Journal of Biological Sciences* 3: 1110-1112.

Nawar, S., Reda, M., Farag, F., El Nahry, A.H., 2011. Mapping soil salinity in El-Tina plain in Egypt using geostatistical approach. Proceedings of the Geoinformatics Forum Salzburg, 5–8 July 2011, Salzburg, Austria.

Negreiros, J., Painho, M., Aguilar, F., Aguilar, M., 2010. Geographical information systems principles of ordinary kriging interpolator. *Journal of Applied Sciences* 10: 852-867.

Nezami, M.T., Alipour, Z.T., 2012. Preparing of the soil salinity map using geostatistics method in the Qazvin Plain. *Journal of Soil Science and Environmental Management* 3(2): 36-41.

Nie, S., Bian, J., Zhou, Y., 2021. Estimating the spatial distribution of soil salinity with geographically weighted regression kriging and ıts relationship to groundwater in the western Jilin Irrigation Area, Northeast China. *Polish Journal of Environmental Studies* 30(1): 283-294.

Panagos, P., Van Liedekerke, M., Jones, A., Montanarella, L., 2012. European soil data centre: Response to European policy support and public data requirements. *Land Use Policy* 29 (2): 329-338.

Panday, D., Maharjan, B., Chalise, D., Shrestha, R.K., Twanabasu, B., 2018. Digital soil mapping in the Bara district of Nepal using kriging tool in ArcGIS. *PloS one* 13(10): e0206350.

Pásztor, L., Laborczi, A., Bakacsi, Z., Szabó, J., Illés, G., 2018. Compilation of a national soil-type map for Hungary by sequential classification methods. *Geoderma* 311: 93–108.

Pásztor, L., Laborczi, A., Takács, K., Szatmári, G., Dobos, E., Illés, G., Bakacsi, Z., Szabó, J., 2015. Compilation of novel and renewed, goal oriented digital soil maps using geostatistical and data mining tools. *Hungarian Geographical Bulletin* 64(1): 49-64.

Pulatov, A., Khamidov, A., Akhmatov, D., Pulatov, B., Vasenev, V., 2020. Soil salinity mapping by different interpolation methods in Mirzaabad district, Syrdarya Province. IOP Conference Series: Materials Science and Engineering, International Scientific Conference Construction Mechanics, Hydraulics and Water Resources Engineering (CONMECHYDRO – 2020) 23-25 April 2020, Tashkent Institute of Irrigation and Agricultural Mechanization Engineers, Tashkent, Uzbekistan, Volume 883, 012089

Ronai, A., 1986. The Quaternary of the Great Hungarian Plain. Available at [Access date: 21.04.2021]: http://epa.oszk.hu/02900/02986/00025/pdf/EPA02986_geologica_hungarica_ser_geol_1985_21_413-445.pdf

Sahbeni, G., 2021. A PLSR model to predict soil salinity using Sentinel-2 MSI data. *Open Geosciences* 13(1): 977-987.

Sahbeni, G., 2021. Soil salinity mapping using Landsat 8 OLI data and regression modeling in the Great Hungarian Plain. *SN Applied Sciences* 3: 587.

Samsonova, V.P., Blagoveshchenskii, Y.N., Meshalkina, Y.L., 2017. Use of empirical Bayesian kriging for revealing heterogeneities in the distribution of organic carbon on agricultural lands. *Eurasian Soil Science* 50: 305–311.

Sangani, M.F., Khojasteh, D.N., Owens, G., 2019. Dataset characteristics influence the performance of different interpolation methods for soil salinity spatial mapping. *Environmental Monitoring and Assessment* 191: 684.

Schofield, R., Thomas, D., Kirkby, M., 2001. Causal processes of soil salinization in Tunisia, Spain, and Hungary. *Land Degradation and Development* 12(2): 163-181.

Scudiero, E., Corwin, D.L., Anderson, R.G., Yemoto, K., Clary, W., Wang, Z., Skaggs, T., 2017. Remote sensing is a viable tool for mapping soil salinity in agricultural lands. *California Agriculture* 71(4):231–238.

Shahid, S.A., Zaman, M., Heng, L., 2018. Soil salinity: Historical perspectives and a world overview of the problem. In: Guideline for salinity assessment, mitigation, and adaptation using nuclear and related techniques. Zaman, M., Shahid, S.A., Heng, L. (Eds.). Springer, Cham. pp 43-53.

Shainberg, I., Rhoades, J.D., Prather, R.J., 1980. Effect of exchangeable sodium percentage, cation exchange capacity, and soil solution concentration on soil electrical conductivity. *Soil Science Society of America Journal* 44(3): 469-473.

Silva, B.B., Braga, A.C., Braga, C.C., Oliveira, L.M., Montenegro, S., Junior, B.B., 2016. Procedures for calculation of the albedo with OLI-Landsat 8 images: Application to the Brazilian semi-arid. *Revista Brasileira de Engenharia Agricola e Ambiental* 20:3-8.

Smith, T.E., 2011. Notebook for spatial data analysis: Part II. Continuous Spatial Data Analysis: 4- Variograms. ESE 502, Available at [Access date: 21.04.2021]: https://www.seas.upenn.edu/~tesmith/NOTEBOOK/Part_II/4_Variograms.pdf

Szabó, J., Pirkó, B., 2017. The Hungarian monitoring system – results weaknesses, development opportunities. The soil information and monitoring system (TIM). Available at [Access date: 21.04.2021]: http://eagri.cz/public/web/file/519224/_2_7_Bela_Pirko.pdf

Szatmári, G., Bakacsi, Z., Laborczi, A., Petrik, O., Pataki, R., Tóth, T., Pásztor, L., 2020. Elaborating Hungarian segment of the global map of salt-affected soils (GSSmap): national contribution to an international initiative. *Remote Sensing* 12(24): 4073.

Taghadosi, M., Hasanlou, M., Eftekhari, K., 2019. Soil salinity mapping using dual-polarized SAR Sentinel-1 imagery. *International Journal of Remote Sensing* 40(1): 237-252.

Tajgardan, T., Ayoubi, S., Shataee, S., Sahrawat, K., 2010. Soil surface salinity prediction using ASTER data: Comparing statistical and geostatistical models. *Australian Journal of Basic and Applied Sciences* 4(3): 457-467.

Thompson, J.A., Roecker, S., Grunwald, S., Owens, P.R., 2012. Digital Soil Mapping: Interactions with and Applications for Hydropedology. In: Hydropedology. Lin, H. (Ed.). Elsevier. pp.665-709.

Tóth, G., Adhikari, K., Várallyay, Gy., Tóth, T., Bódis, K., Stolbovoy, V., 2008. Updated map of salt-affected soils in the European Union. In: Threats to Soil Quality in Europe. EUR 23438 EN. Tóth, G., Montanarella, L., Rusco, E. (Eds). European Commission, Joint Research Centre, Institute for Environment and Sustainability Office of Official Publications of the European Communities. Luxembourg, pp. 65–77. Available at [Access date: 21.04.2021]: https://esdac.jrc.ec.europa.eu/ESDB_Archive/eusoils_docs/other/EUR23438.pdf

Tóth, T., 2009. Monitoring, predicting and quantifying soil salinity, sodicity and alkalinity in Hungary at different scales: Past experiences, current achievements and outlook with special regard to European Union initiatives, Advances in the assessment and monitoring of salinization and status of biosaline agriculture. Report of an expert consultation held in Dubai, United Arab Emirates, 26-29 November 2007. World Soil Resources Report. No 104. FAO, Rome, Italy. Available at [Access date: 21.04.2021]: https://tibortothsoil.members.iif.hu/abstr/T2009.pdf

Tóth, T., Balog, K., Szabo, A., Pásztor, L., Jobbágy, E.G., Nosetto, M.D., Gribovszki, Z., 2014. Influence of lowland forests on subsurface salt accumulation in shallow groundwater areas. *AoB PLANTS* 6: plu054.

Tóth, T., Pásztor, L., Kabos, S., Kuti, L., 2002. Statistical prediction of the presence of salt-affected soils by using digitalized hydrogeological maps. *Arid Land Research and Management* 16(1):55–68.

Triantafilis, J., Odeh, I., McBratney, A., 2001. Five geostatistical models to predict soil salinity from electromagnetic ınduction data across ırrigated cotton. *Soil Science Society of America Journal* 65(3): 869-878.

Tziachris, P., Metaxa, E., Papadopoulos, F., & Papadopoulou, M., 2017. Spatial modelling and prediction assessment of soil iron using kriging interpolation with pH as auxiliary iformation. *International Journal of Geo-Information* 6(9): 283.

Uri, N., 2018. Cropland soil salinization and associated hydrology: trends, processes, and examples. *Water* 10(8): 1030.

Wackernagel, H., 1995. Ordinary Kriging. In: Multivariate Geostatistics. Wackernagel, H. (Ed.). Springer, Berlin, Heidelberg. pp. 74-81.

Wackernagel, H., 2013. Basics in Geostatistics 2 Geostatistical interpolation/estimation: Kriging methods. MINES ParisTech. Available at [Access date:21.04.2021]: https://www.nersc.no/sites/www.nersc.no/files/Basics2kriging.pdf

Xiao, Y., Gu, X., Yin, S., et al., 2016. Geostatistical interpolation model selection based on ArcGIS and Spatio-temporal variability analysis of groundwater level in piedmont plains, northwest China. *SpringerPlus* 5: 425.

Zhang, Y., 2011. Introduction to Geostatistics-Course Notes. University of Wyoming. 31p. Available at [Access date: 21.04.2021]: http://www.uwyo.edu/geolgeophys/people/faculty/yzhang/_files/docs/geosta1.pdf

Zheng, Z., & Zhang, F., & Chai, X., Zhu, Z., Ma, F., 2009. Spatial estimation of soil moisture and salinity with neural kriging. International Conference on Computer and Computing Technologies in Agriculture. CCTA 2008: Computer and Computing Technologies in Agriculture II, IFIP Advances in Information and Communication Technology, Vol 294. Springer, Boston, MA. pp. 1227-1237.